AIAA JOURNAL
Vol. 44, No. 12, December 2006

Evaluation of Detached Eddy Simulation for Turbulent Wake Applications

Matthew F. Barone*
Sandia National Laboratories, Albuquerque, New Mexico 87185
and
Christopher J. Roy†
Auburn University, Auburn, Alabama 36849

DOI: 10.2514/1.22359

Simulations of a low-speed square cylinder wake and a supersonic axisymmetric base wake are performed using the detached eddy simulation model. A reduced-dissipation form of a shock-capturing flux scheme is employed to mitigate the effects of dissipative error in regions of smooth flow. The reduced-dissipation scheme is demonstrated on a two-dimensional square cylinder wake problem, showing a marked improvement in accuracy for a given grid resolution. The results for simulations on three grids of increasing resolution for the three-dimensional square cylinder wake are compared with experimental data and to other computational studies. The comparisons of mean flow and global flow quantities to experimental data are favorable, whereas the results for second order statistics in the wake are mixed and do not always improve with increasing spatial resolution. Comparisons to large eddy simulation are also generally favorable, suggesting detached eddy simulation provides an adequate subgrid scale model. Predictions of base drag and centerline wake velocity for the supersonic wake are also good, given sufficient grid refinement. These cases add to the validation library for detached eddy simulation and support its use as an engineering analysis tool for accurate prediction of global flow quantities and mean flow properties.

Nomenclature

A	=	cylinder aspect ratio
C_{DES}	=	detached eddy simulation model constant
C_d	=	drag coefficient
C_l	=	lift coefficient
C_{p_b}	=	base pressure coefficient
D	=	square cylinder width
d	=	distance to wall
$\boldsymbol{F}_j$	=	inviscid flux vector
l_R	=	wake recirculation length
M	=	Mach number
N	=	number of grid cells
p	=	pressure
Q_j^l	=	flux limiter
R	=	axisymmetric base radius
R_j	=	matrix of right eigenvectors
Re	=	Reynolds number
r	=	radial coordinate
Sr	=	Strouhal number
T	=	total simulation time, temperature
t_c	=	characteristic time
$\boldsymbol{U}_j$	=	conservative variable vector
U_∞	=	freestream velocity
u, v, w	=	velocity components
α_j^l	=	characteristic variables
Δt	=	time step
$\Delta x, \Delta y, \Delta z, \Delta r$	=	grid spacings
δ	=	boundary layer thickness
θ	=	azimuthal coordinate
θ_j^l	=	artificial compression method switch
κ	=	numerical dissipation parameter
λ_j^l	=	flux Jacobian eigenvalues
$\boldsymbol{\Phi}_j$	=	Roe dissipation vector
ϕ_j^l	=	element of $\boldsymbol{\Phi}_j$
$\langle\,\rangle$	=	time-averaged quantity

Subscript

∞	=	freestream quantity

Superscripts

l	=	lth element
$+$	=	near-wall viscous scaling
$'$	=	fluctuation quantity

I. Introduction

VALIDATION of closure models for the Reynolds-averaged Navier–Stokes (RANS) equations has been an ongoing effort for several decades. Some of the more popular algebraic, one-equation, and two-equation models have been tested on a wide variety of turbulent flows by many different researchers (see, e.g., Kline et al. [1] and Bradshaw et al. [2]). These validation efforts are the key to obtaining a good description of the validity, accuracy, and utility of the various models over a range of applications. Testing of the models by independent workers is particularly important.

Flows involving massive separation and/or turbulent flow structure that scales with vehicle or obstacle size comprise an especially difficult class of problems for RANS models. As available computing capacity increases, computational fluid dynamics (CFD) researchers and practitioners are moving towards the use of large eddy simulation (LES) as a higher fidelity alternative to RANS. LES suffers from stringent near-wall spatial resolution requirements, and so a practical alternative that seeks to leverage the best qualities of RANS and LES is the so-called hybrid RANS/LES method. Generally speaking, a hybrid RANS/LES model applies a RANS closure model in the attached boundary layer region and a LES

Presented as Paper 0504 at the 43rd AIAA Aerospace Sciences Meeting and Exhibit, Reno, NV, 10–13 January 2005; received 9 January 2006; revision received 15 June 2006; accepted for publication 24 July 2006.

*Aerosciences and Compressible Fluid Mechanics Department, Mail Stop 0825. Member AIAA.
†Assistant Professor, Aerospace Engineering Department. Senior Member AIAA.

subgrid-scale model in regions of massively separated flow. The equations of motion are usually, but not necessarily, integrated in a time-accurate way for both the RANS and LES regions. The RANS and LES regions may be delineated using a zonal scheme or a smooth blending parameter.

The validation of hybrid RANS/LES models is a tricky subject. RANS models are amenable to the usual verification/validation sequence [3]; solution verification (grid refinement and iterative convergence criteria) is performed to assess numerical error in the solution. Then the model error may be assessed without complication. Conventional LES techniques are inherently difficult to verify and validate. Usually, the filter width is related to the grid spacing so that, as the grid is refined, the model and therefore, the solution, are also refined. This occurs simultaneously with numerical error reduction. The grid-refinement limit becomes direct numerical simulation which is, of course, impracticable for most flows of interest. Fixing the filter width and then applying grid refinement is a possible solution, but this strategy can be expensive and difficult to apply to complex geometries.

In the present work, we take a less rigorous view of the model validation process, akin to previous efforts applied to RANS closure models. Benchmark problems are identified that 1) have reliable experimental data sets for comparison, and 2) others have attempted to simulate using the same or similar models but possibly different numerical techniques. Well-documented simulation results are added to the knowledge database for these problems so that educated decisions may be made regarding application of the model to similar problems of engineering interest.

The focus of this paper is the application of the detached eddy simulation (DES) model to the bluff body wake. DES is perhaps the most popular hybrid RANS/LES model currently in use. Initial work on this problem, including detailed studies of the effects of numerics, grid convergence, and iterative convergence, was begun by Roy et al. [4]. In the current work, two three-dimensional problems are examined: 1) the wake of a square cylinder in low-speed flow, and 2) the wake behind an axisymmetric base in supersonic flow.

II. Simulation Methodology

A. Numerical Method

Most production CFD codes used for compressible flow problems are based on schemes of second order accuracy in space, with some form of numerical dissipation incorporated for numerical stability and to accommodate solution discontinuities. Although accurate results for unsteady turbulent flows are possible with such schemes, the required grid size may be prohibitively large. This is primarily due to excessive artificial diffusion of the energy-containing turbulent eddies by the numerical scheme. Several methods for switching off the dissipation operators in LES regions and/or regions of smooth flow have been proposed. Here we use the scheme of Yee et al. [5], which is implemented simply and naturally in a wide range of shock-capturing schemes that employ characteristic-based numerical diffusion. This scheme uses the artificial compression method (ACM) switch of Harten [6], which senses the severity of gradients of characteristic variables, and scales the magnitude of the numerical diffusion operating on each characteristic wave accordingly.

In this work, a structured grid, finite volume compressible flow solver, the Sandia Advanced Code for Compressible Aerothermodynamics Research and Analysis [7,8], was modified to incorporate the ACM switch into the existing symmetric total variation diminishing (STVD) scheme of Yee [9]. Following the nomenclature of Yee et al. [5], the modified scheme is called the ACMSTVD scheme throughout the rest of this paper.

The STVD flux scheme uses the Roe flux, which may be written as the sum of a centered approximation and a dissipation term

$$\boldsymbol{F}_{j+1/2} = \frac{\boldsymbol{F}_j + \boldsymbol{F}_{j+1}}{2} + \frac{1}{2} R_{j+1/2} \boldsymbol{\Phi}_{j+1/2} \tag{1}$$

$R_{j+1/2}$ is the matrix of right eigenvectors of the Jacobian $\partial F/\partial \boldsymbol{U}_{j+1/2}$, and $\boldsymbol{\Phi}_{j+1/2}$ is the dissipation operator acting across the face separating volumes j and $j+1$. The elements of the vector $\boldsymbol{\Phi}_{j+1/2}$ in the STVD scheme are written as

$$\phi^l_{j+1/2} = -\left|\lambda^l_{j+1/2}\right|\left(\alpha^l_{j+1/2} - Q^l_{j+1/2}\right) \tag{2}$$

where

$$\alpha^l_{j+1/2} = \left[R^{-1}_{j+1/2}(\boldsymbol{U}_{j+1} - \boldsymbol{U}_j)\right]^l \tag{3}$$

are the characteristic variables and Q is the minmod limiter

$$Q^l_{j+1/2} = \text{minmod}\left(\alpha^l_{j-1/2}, \alpha^l_{j+1/2}, \alpha^l_{j+3/2}\right) \tag{4}$$

The low-dissipation scheme is constructed by replacing the elements of the dissipation vector $\boldsymbol{\Phi}_{j+1/2}$ with modified entries of the form

$$\phi^{l*}_{j+1/2} = \kappa \theta^l_{j+1/2} \phi^l_{j+1/2} \tag{5}$$

The constant $0 \le \kappa \le 1$ globally reduces the magnitude of the dissipative portion of the flux. The numerical dissipation may be further reduced through the action of the ACM switch

$$\theta^l_{j+1/2} = \frac{\left|\alpha^l_{j+1/2} - \alpha^l_{j-1/2}\right|}{\left|\alpha^l_{j+1/2}\right| + \left|\alpha^l_{j-1/2}\right|} \tag{6}$$

which serves as a flow gradient sensor. In the vicinity of a shock wave or contact discontinuity, the original STVD scheme is applied (modified by the global constant κ), whereas in regions of smooth flow the numerical dissipation is reduced. Coupling the strength of numerical dissipation to the behavior of characteristic variables tunes the dissipation operator to the relevant local physics. In practice, Yee et al. [5] obtained nonoscillatory solutions for problems with shock waves using $0.35 \le \kappa \le 0.70$.

B. Detached Eddy Simulation

The DES model, proposed by Spalart et al. [10], is built upon the one-equation Spalart–Allmaras (SA) RANS closure model [11]. The eddy viscosity term in this model contains a destruction term that depends upon the distance to the nearest solid wall. The DES model applies the SA model with one simple modification: the distance to the wall d is replaced by a length scale that is the lesser of d and a length proportional to the local grid spacing Δ

$$d = \min(C_{\text{DES}}\Delta, d), \qquad \Delta = \max(\Delta x, \Delta y, \Delta z) \tag{7}$$

The constant C_{DES} is set to 0.65 based on a calibration in isotropic turbulence. The switch (7) provides a transition from the RANS model near the solid wall to the LES region away from the wall. In the LES region, the eddy viscosity serves as a Smagorinsky-type subgrid-scale model for the action of the unresolved turbulent motions.

III. Results

A. Demonstration of the Low-Dissipation ACMSTVD Scheme

The advantages of the ACMSTVD scheme over the baseline STVD scheme are exemplified by application of the two schemes to flow past a square cylinder at a Reynolds number Re_D of 21,400 and freestream Mach number of 0.1. In this numerical test case the flow is artificially restricted to two spatial dimensions to reduce computational cost and allow quick turnaround for multiple calculations. The DES hybrid model described in Sec. II.B is employed in this study. A schematic of the computational domain is shown in Fig. 1.

Figure 2a shows the mean centerline ($y = 0$) streamwise velocity in the cylinder wake using the baseline STVD scheme compared with results obtained with the reduced-dissipation ACMSTVD scheme. A similar comparison of the rms streamwise velocity fluctuations is made in Fig. 2b. Solutions using the STVD scheme were obtained on

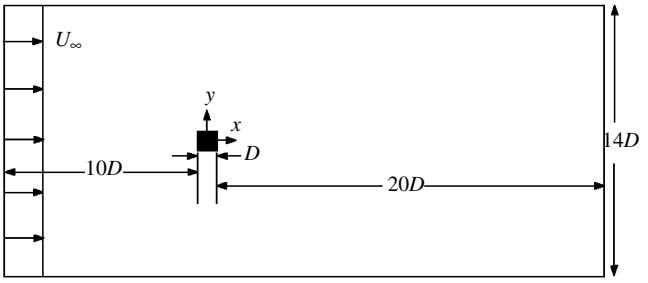

Fig. 1 Schematic of the computational domain for the square cylinder wake simulations.

a coarse grid (10,000 cells) and a fine grid (160,000 cells), with the fine-grid solution estimated to be nearly grid-converged based on the results for this problem given in Roy et al. [4]. The ACMSTVD solutions were only obtained on the coarse grid. The parameter κ allows global reduction of the numerical dissipation, whereas the ACM switch only reduces the dissipation at sharp gradients; for $\kappa = 1.0$ the amount of dissipation applied at a shock is nominally the same as that of the baseline scheme. As κ is reduced, numerical stability is maintained and agreement with the fine-grid reference solution improves dramatically.

Table 1 shows the improvement in prediction of global flow metrics as the amount of numerical dissipation decreases with decreasing κ. Here $\langle C_d \rangle$ is the time-averaged drag coefficient, $C'_{d_{\text{rms}}}$ and $C'_{l_{\text{rms}}}$ are the rms drag and lift fluctuations, and l_R is the wake recirculation length. Note that, for a given grid resolution, the increase in accuracy obtained by using the ACMSTVD scheme is gained at a computational cost increase of approximately 5% over the baseline STVD scheme.

Table 1 Comparison of global quantities for the 2D square cylinder problem

Grid	Method	$\langle C_d \rangle$	l_R/D	$C'_{d_{\text{rms}}}$	$C'_{l_{\text{rms}}}$
Coarse	STVD	1.57	2.43	0.02	0.10
Coarse	ACMSTVD, $\kappa = 1.00$	1.58	2.00	0.06	0.36
Coarse	ACMSTVD, $\kappa = 0.70$	1.73	1.62	0.21	1.00
Coarse	ACMSTVD, $\kappa = 0.35$	2.20	1.05	0.45	1.29
Coarse	ACMSTVD, $\kappa = 0.20$	2.28	1.12	0.52	1.33
Fine	STVD	2.40	1.22	0.65	1.26

B. Turbulent Wake of a Square Cylinder

The first validation case considered is the low-speed flow past a square cylinder of width D. A cross section of the problem geometry is pictured in Fig. 1. In the three-dimensional problem the cylinder has finite extent in the spanwise, or z, direction. The flow conditions are chosen to match the water tunnel experiment of Lyn et al. [12]. The compressible flow equations are solved with air as the medium, necessitating simulations at a finite Mach number; we choose a nominal freestream Mach number of 0.1, so that the flow is incompressible in character throughout the domain. The viscosity is set to match the experimental Reynolds number based on cylinder width of 21,400. The dimensions of the computational domain are also shown in Fig. 1. The spanwise extent of the domain is $4D$, which has become a somewhat standard value for numerical studies of this problem [13,14]. At the inflow boundary, stagnation pressure and stagnation temperature are specified to provide a uniform oncoming flow. The spanwise boundaries are periodic, whereas a constant pressure boundary condition is applied at the outflow.

This problem was solved by many LES practitioners as part of two LES workshops [13,14]. The results were mixed and disappointing in the sense that no single simulation gave accurate results for all flow quantities considered. Since then, at least two LES studies have been performed with better results [15,16]. We compare some of the results of this work to the LES results of Sohankar et al. [15], who used a second order centered difference scheme along with a second order temporal scheme to simulate the incompressible square cylinder wake at $Re_D = 21,000$. Several subgrid models were investigated, with the best overall results obtained using a one-equation dynamic Smagorinsky model on a fine grid containing 1,013,760 cells (case OEDSMF). We include comparisons for some global flow quantities to one of the LES results reported by Fureby et al. [16]. The particular case selected for comparison is a constant-coefficient Smagorinsky LES performed on a 518,400 cell mesh and an extended domain spanning 8 cylinder diameters in the spanwise direction. Finally, we make some comparisons to the results of Schmidt and Thiele [17], who also used the DES model to simulate the square cylinder wake. The grids in their study were purposefully coarse to test the limits of the method. Here we compare only to their finest grid case, which used about 640,000 grid cells (case DES-A).

There are three classes of quantities that may be used to compare simulation results with the experimental data. The first set is composed of global quantities, including the time-averaged drag on the cylinder, the Strouhal number of the dominant shedding mode, the recirculation length, and the rms lift and drag fluctuations. It is not easy to predict all of the global quantities well, although the more recent LES studies do this reasonably well. The second set of data for comparison is the mean flow, particularly in the near-wake region. Lastly, for a sufficiently resolved flow, one may compare the components of the Reynolds stresses. In this paper, the notation for describing the time-averaged and fluctuating decomposition of a signal is $u = \langle u \rangle + u'$. The terminology "mean" and "time-averaged" are also used interchangeably.

The simulation parameters for the present square cylinder wake calculations are given in Table 2. N_{xy} is the number of grid cells in an x–y plane, whereas N_z is the number of cells in the spanwise direction. $\Delta y_{\min}$ is the cross-stream grid spacing at $x = 0$, $y/D = \pm 0.5$, and Δy_{cl} is the spacing at $x = 0$, $y = 0$. An x–y slice through the near-field region of the medium grid is shown in Fig. 3. The RANS region extended from 4 to 12 grid cells from the cylinder on each grid. The square cylinder flow separates at the forward corners, so that there are no attached turbulent boundary layers present. Thus, this problem is a test of the LES capabilities of DES

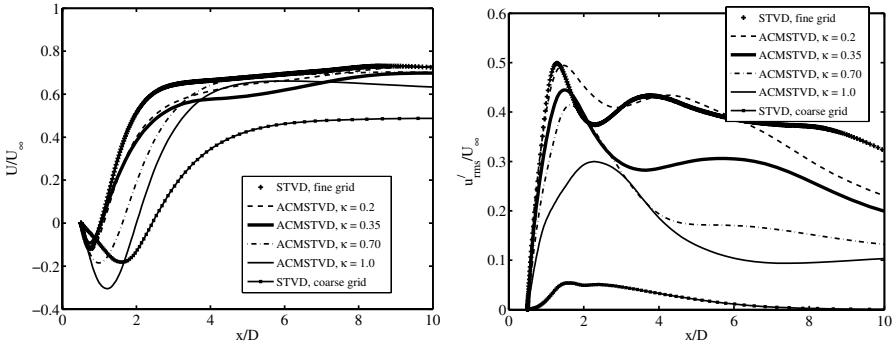

a) Mean streamwise velocity distribution **b) RMS streamwise velocity fluctuation**

Fig. 2 Distribution and fluctuation along the centerline of the 2-D square cylinder wake.

Table 2 Simulation parameters for the square cylinder simulations

Grid	N_{xy}	N_z	N	$\Delta y_{\min}/D$	$\Delta y_{cl}/D$	$\Delta t/t_c$	T/t_c
Coarse	9800	32	313,600	0.0105	0.095	0.0032	256
Medium	39,200	64	2,508,000	5.05×10^{-3}	0.048	0.0032	243.2
Fine	88,200	96	8,467,200	3.4×10^{-3}	0.032	0.0032	253.1

and the ability of DES to properly generate eddy viscosity in the initial shear layers so that the proper downstream wake dynamics are captured.

All three simulations were computed using the ACMSTVD scheme with $\kappa = 0.35$. The time step and the number of subiterations per time step were chosen based on the results of a temporal convergence study performed by Roy et al. [4] on the two-dimensional version of this flow. The number of subiterations per time step was set to ten, enough to reduce the momentum residual magnitude by 2.5 to 3.5 orders of magnitude per time step. The simulations were run for a total time of T seconds; the simulation times are normalized by the characteristic flow time $t_c = D/U_\infty$ in the table. One vortex shedding period corresponds to approximately 7.7 characteristic flow times. Flow variable sampling was initiated after a transient period of about 32 characteristic times and samples were taken every 10 time steps, such that the sampling resolved frequencies up to about 200 times that of the vortex shedding frequency. Data were sampled along the wake centerline at $y = z = 0$ and at two downstream locations, $x/D = 1$ and $x/D = 5$. The data were not spanwise-averaged, but the sampling times were long enough to provide statistically converged quantities.

The lift and drag histories were also recorded for each simulation. Figure 4a shows the time history of the drag coefficient for the coarse-grid solution, along with the running average[‡] beginning at $t/t_c = 31.4$. A measure of the degree of statistical convergence is given by the maximum deviation of the drag coefficient running average from its final value over the final 50 characteristic times. The deviations were 0.22, 0.40, and 0.64% for the coarse, medium, and fine grids, respectively. The drag histories for the fine and medium grids are show in Figs. 4b and 5a. The fine-grid drag history is distinct in that it contains a somewhat regular low-frequency component mostly absent in the other two results. It is not clear whether this solution behavior is physical or an artifact of the simulation. The most likely cause of artificial low-frequency forcing is interaction of the flow with the boundary conditions. At the downstream boundary, vortices convecting out of the domain become stronger and better resolved as the grid is refined, increasing the chances of spurious interaction with the outflow boundary condition. Unfortunately, the high cost of the fine-grid simulations precludes us from studying the effect of up- and downstream boundary placement. As will be shown, the fine-grid results are mostly superior to the results on the other grids, with the exception of rms drag fluctuation and an overprediction of streamwise velocity fluctuation in the near-wake.

Demonstration of statistical convergence is further illustrated in Fig. 5b, which shows time-averaged centerline velocity distributions in the near-wake region for several different sampling periods on the medium grid. This result shows that the wake velocity distribution is sufficiently converged by 210 characteristic flow times. Similar results are observed for simulations on the other two grids.

After the simulations were run, it was discovered that the character of the prescribed inflow was different than the intended result. The source of the discrepancy was the fact that the inflow boundary condition was prescribed as a constant stagnation pressure and stagnation temperature condition. The static pressure perturbation caused by the presence of the cylinder extended upstream to the inflow boundary, resulting in an elevated pressure and diminished freestream velocity. The uniformity of the inflow velocity was not substantially altered. However, the freestream velocity is an important normalization parameter for the quantities of interest and must be known accurately. The following procedure ensured a good estimate of the true freestream velocity. The flow was assumed to be incompressible, resulting in negligible density changes. The mean mass flux across a plane at $x = 1$ and at $x = 5$ was computed. The mean of the area-averaged mass flux divided by the density at the two planes was taken to be the freestream velocity value. The freestream velocities derived in this manner at the two planes differed by less than 0.5% in each case considered. This is similar to the method carried out by Lyn et al. [12] to determine the oncoming velocity in the experiments.

A further consideration for comparing simulation results to experiments is the effect of blockage. This issue is discussed in some detail in Sohankar et al. [15]. Here, we use the bluff body blockage corrections of Maskell [18] for mean drag coefficient, rms lift coefficient, and rms drag coefficient fluctuations. The Strouhal number is corrected according to the method described in Sohankar et al. [15]. The blockage corrections allow comparison of global quantities across experiments with different tunnel configurations. Blockage corrections for the present DES simulations were roughly 11% for the force coefficients and 4% for the Strouhal number. The corrections resulted in a decrease in the force coefficients and in the Strouhal number for all the simulations. Note that not all the experiments reported enough information to apply the correction; these are noted as "uncorrected" in the table of results to follow.

The predictions for global quantities are compared with the selected LES simulations and to experimental values in Table 3. Force coefficient and Strouhal number values are corrected for blockage unless otherwise noted. Table 4 gives the percent error of the DES simulation predictions relative to the average of the available experimental results. The Strouhal number is well predicted by the fine-grid DES and by the LES simulations, whereas the coarser DES simulations give a slight underprediction. Note that with application of the blockage correction, the DES results of Schmidt and Thiele [17] and the LES results of Fureby et al. [16] would also likely underpredict the Strouhal number. Mean drag coefficient is well predicted by all simulations with the exception of the DES-A calculation; application of a blockage correction would likely improve that particular result. Recirculation length prediction improves dramatically with grid refinement, with the fine-grid result within 3% of the experimental value.

The present DES predictions of rms drag coefficient fluctuation increase with improving resolution, exhibiting worsening agreement with the single experimental value. It is assumed here that the rms lift

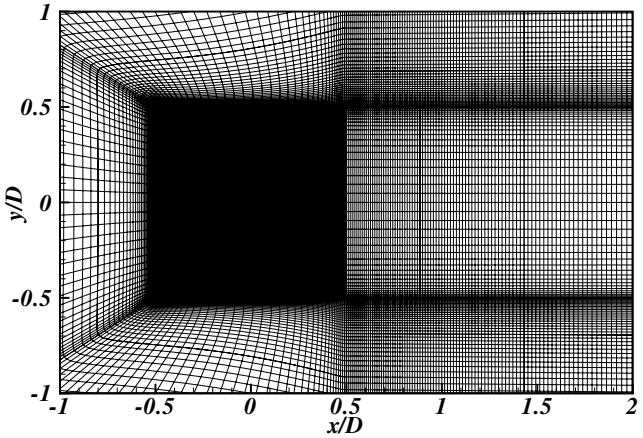

Fig. 3 Near field of a constant-z surface of the medium grid.

[‡]The running average is the average of the first i samples, computed for $i = 1, 2, \ldots, N_{\text{samples}}$

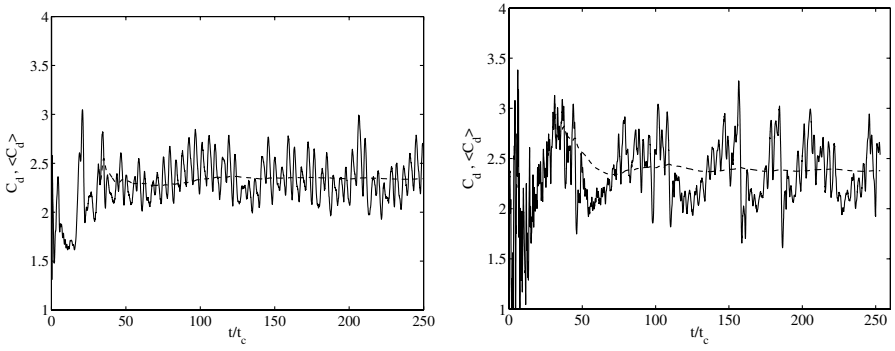

a) Coarse grid **b) Fine grid**

Fig. 4 Uncorrected instantaneous drag and mean drag convergence history for square cylinder simulations.

and drag fluctuations are relatively insensitive to the Reynolds number [15]. Note that the reported experimental rms drag coefficient is a sectional value, measured at a single spanwise location. In the simulations, the forces are computed over the entire cylinder, i.e., integrated along the span. The rms drag fluctuation on the entire cylinder is somewhat less than the sectional drag due to imperfect correlation of the sectional drag signals; Sohankar et al. [15] reported a ratio of about 0.7. The sectional rms drag fluctuation is, therefore, overpredicted by as much as 100% by the fine-grid DES simulation. This may be due to the aforementioned low-frequency oscillations observed in the fine-grid drag history, although the Sohankar LES similarly overpredicts the rms drag fluctuations. The rms lift fluctuation is much better correlated along the length of the cylinder so that the sectional and spanwise-averaged values are very close to one another. RMS lift coefficient fluctuations are not terribly sensitive to choice of grid or subgrid model, with agreement to within 10% of the averaged experimental value.

In summary, the present medium and fine-grid DES results are competitive with the LES calculations in predictions of global quantities. Further refinement of the DES grid leads to only marginal improvements in Strouhal number and mean drag coefficient prediction, and significant improvement in the recirculation length prediction. Fluctuations in the lift agree well with the experimental values, whereas the drag fluctuation prediction on the fine grid deviates from the experimental average by more than 40% and worsens with increasing grid resolution.

DES predictions of the mean streamwise velocity and rms velocity fluctuations along the wake centerline are shown in Figs. 6 and 7. Prediction of the mean streamwise velocity in the near-wake improves with increasing grid resolution. Further downstream the coarse and medium grids both overpredict the level of wake recovery, whereas the fine grid agrees well with the experimental data. The medium-grid predictions of u'_{rms} are in excellent agreement with the experiment, whereas the coarse grid gives values that are up to 40% low. The fine grid overpredicts the peak in u'_{rms} near $x/D = 1.5$, however, this discrepancy does not appear to adversely affect predictions of the recirculation length. The medium and fine-grid simulations do very well predicting the dominant velocity fluctuation component v', with the coarse grid overpredicting this quantity for $x/D > 3$. Experimental data are not available for w'_{rms}, but the simulation results show a significant dependence of w'_{rms} on the grid resolution.

The mean velocity and rms velocity fluctuation predictions at $x/D = 1$ are shown in Figs. 8 and 9. Predictions of $\langle u \rangle$ and u'_{rms} generally improve with increasing grid resolution. Prediction of the mean cross-stream velocity $\langle v \rangle$ improves from the coarse to medium grid, but the magnitude of the peak value given by the fine grid is substantially lower than both the other two simulations and the experiment. Surprisingly, the fluctuating cross-stream velocity prediction does not improve from the coarse to the medium grid, with marginal improvements observed in the fine-grid simulation.

Figure 10a shows the Reynolds shear stress at $x/D = 1$. The coarse-grid simulation predicts the peak value well, but not the secondary peak near $y = 0$. The medium and fine-grid simulations significantly overpredict the peak value and do not capture a secondary peak at all. It appears that the DES model with the present numerical scheme is not able to give accurate predictions of Reynolds shear stress in the near-wake. Overall agreement for mean and fluctuating velocities is generally good, however. Figure 10b shows the time-averaged subgrid component of the Reynolds shear stress at $x/D = 1$. Note the reduced scale of the axis in the plot of the subgrid component relative to that of the resolved component. The

Table 4 Percent error in DES simulation predictions relative to average of experimental values

	Sr	$\langle C_d \rangle$	l_R/D	$C'_{d_{\text{rms}}}$	$C'_{l_{\text{rms}}}$
Coarse	−7.1	−2.3	−37.7	−5.6	8.4
Medium	−6.3	−4.2	−16.7	16.7	−2.2
Fine	−4.0	−0.9	2.9	44.4	−6.2

Table 3 Comparison of global quantities for the square cylinder problem

	$Re_D/10^3$	A	Sr	$\langle C_d \rangle$	l_R/D	$C'_{d_{\text{rms}}}$	$C'_{l_{\text{rms}}}$
Numerical Simulations							
DES coarse	19.6	4	0.121	2.08	0.86	0.17	1.34
DES medium	19.7	4	0.122	2.04	1.15	0.21	1.21
DES fine	19.4	4	0.125	2.11	1.42	0.26	1.16
Schmidt and Thiele [17] (DES-A), uncorrected	22.4	4	0.13	2.42	1.16	0.28	1.55
Sohankar et al. [15] (OEDSMF LES)	22	4	0.128	2.09	1.07	0.27	1.40
Fureby et al. [16] (SM LES), uncorrected	21.4	8	0.131	2.1	1.25	0.17	1.30
Experiments							
Lyn et al. [12], uncorrected	21.4	9.8	0.13	2.10	1.38	——	——
Norberg [19]	22	51	0.131	2.11	——	——	——
Bearman/Obasaju [20]	22	17	0.13	2.1	——	——	1.2
McLean/Gartshore [21], uncorrected	16	23	——	——	——	——	1.3
Luo et al. [22]	34	9.2	0.13	2.21	——	0.18	1.21

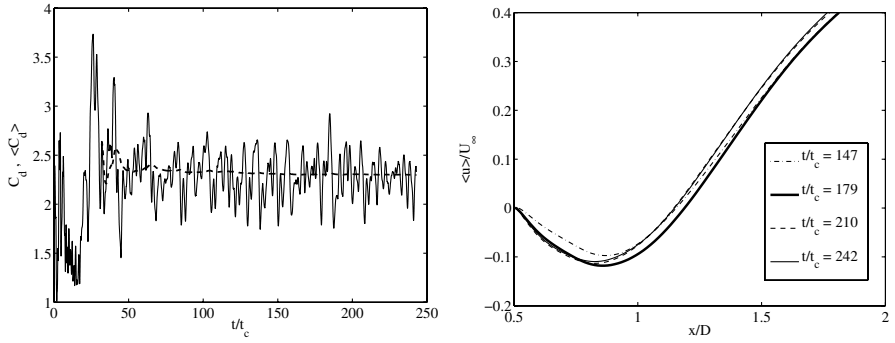

a) Mean drag history **b) Streamwise velocity profile**

Fig. 5 Convergence history for the medium-grid square cylinder simulation.

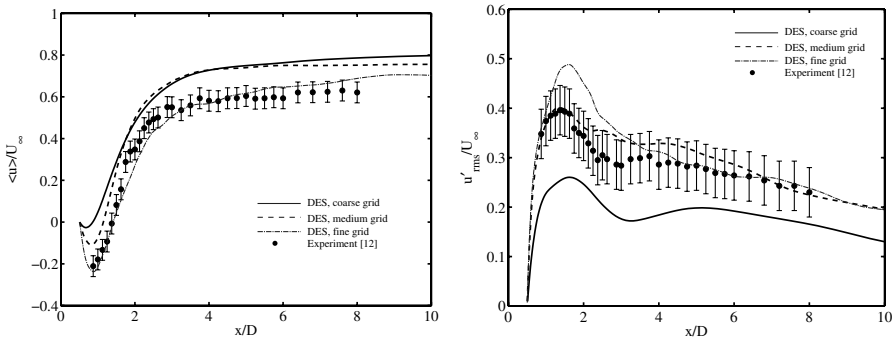

a) Mean streamwise velocity **b) RMS streamwise velocity**

Fig. 6 Mean streamwise velocity and rms streamwise velocity fluctuation along the wake centerline.

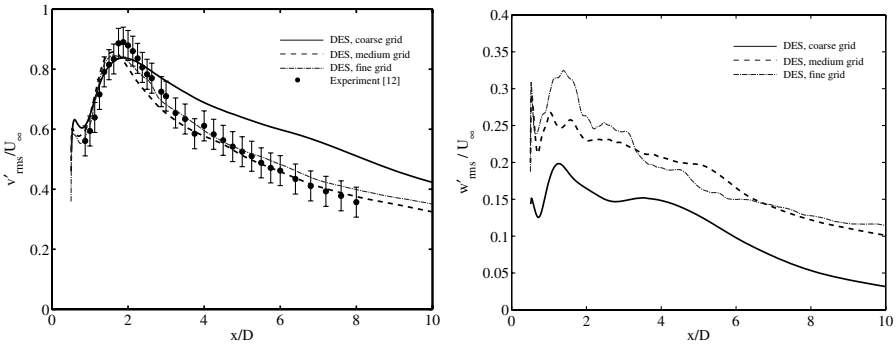

a) RMS cross-stream velocity **b) RMS spanwise velocity**

Fig. 7 Velocity fluctuations along the wake centerline.

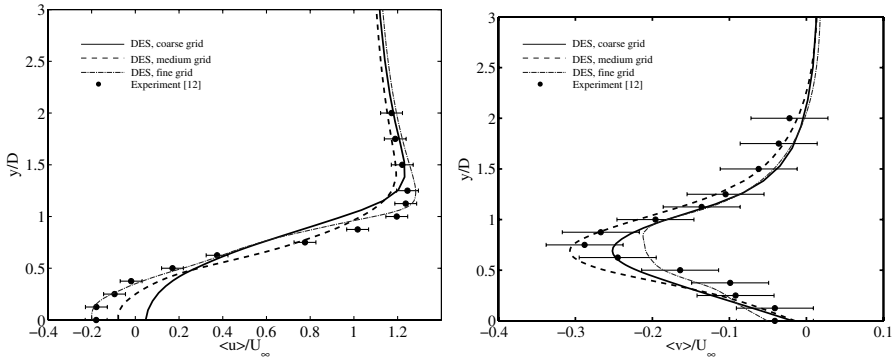

a) Mean streamwise velocity **b) Mean cross-stream velocity**

Fig. 8 Mean streamwise and mean cross-stream velocity at $x/D = 1$.

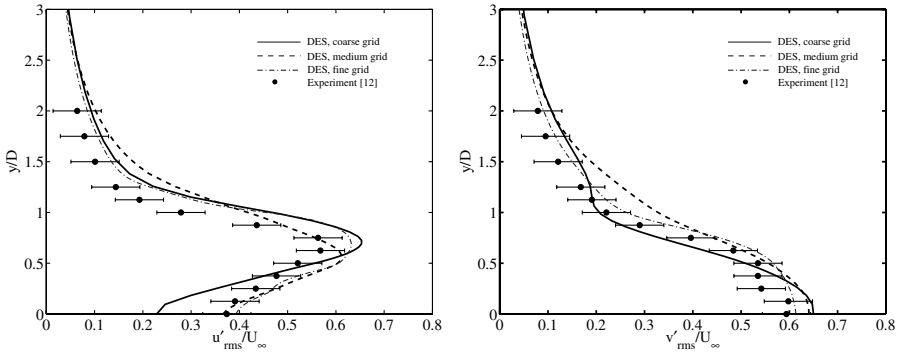

a) RMS streamwise velocity **b) RMS cross-stream velocity**

Fig. 9 RMS streamwise and RMS cross-stream velocity fluctuations at $x/D = 1$.

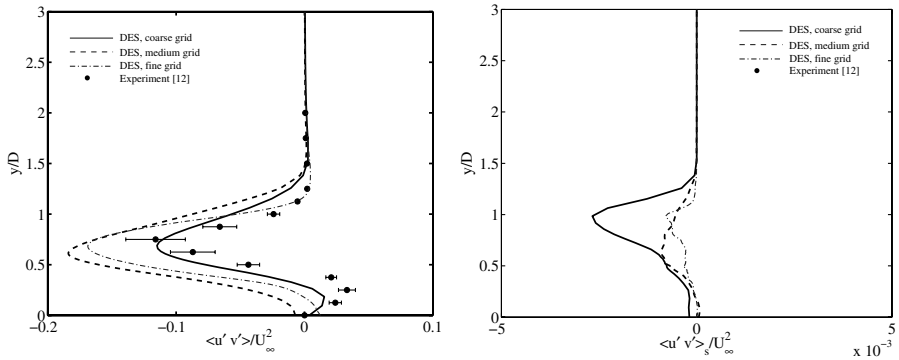

a) Resolved shear stress **b) Subgrid shear stress**

Fig. 10 Resolved and subgrid Reynolds shear stress at $x/D = 1$.

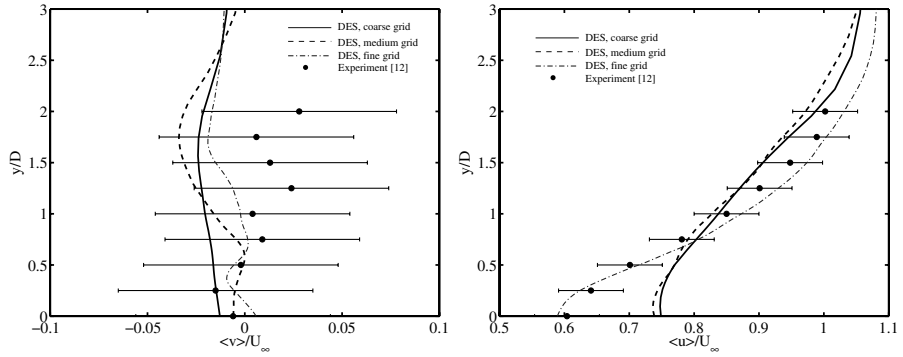

a) Mean cross-stream velocity **b) Mean streamwise velocity**

Fig. 11 Mean cross-stream and streamwise velocity at $x/D = 5$.

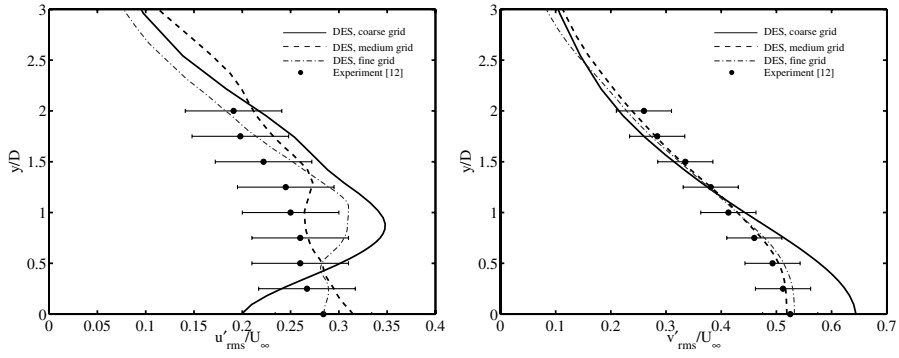

a) RMS streamwise velocity **b) RMS cross-stream velocity**

Fig. 12 RMS streamwise and cross-stream velocity fluctuation at $x/D = 5$.

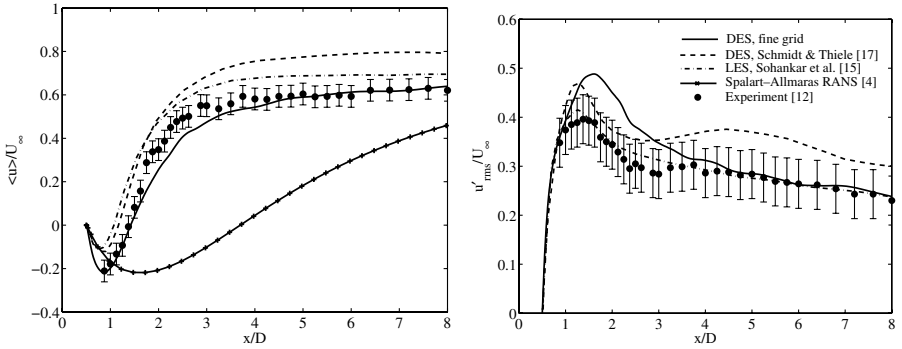

a) Mean velocity distribution **b) RMS velocity fluctuation**

Fig. 13 Mean streamwise velocity distribution and RMS streamwise velocity fluctuation along the wake centerline.

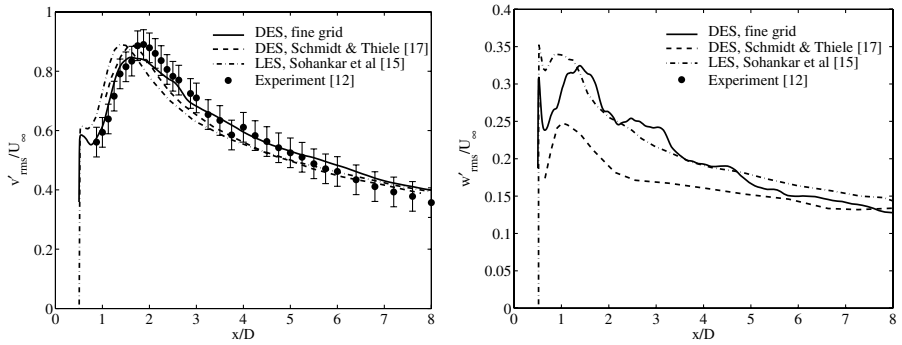

a) RMS cross-stream velocity **b) RMS spanwise velocity**

Fig. 14 RMS cross-stream and spanwise velocity fluctuations along the wake centerline.

peak in the subgrid stress is much larger for the coarse-grid simulation than for the other two grids. The medium and fine-grid results give similar peak values of the subgrid stress but differ in the distribution.

Figures 11 and 12, give results further downstream at $x/D = 5$. Figure 11 shows that the coarse and medium grids overpredict the streamwise velocity recovery, consistent with the results of Fig. 6, whereas the fine-grid result agrees well with experiment. The mean cross-stream velocity at this location is small, and all three simulations give reasonable levels of this quantity. The rms velocity fluctuations are not well predicted on the coarse grid, whereas the medium and fine-grid results are much improved. The Reynolds shear stress is also small at this streamwise location; all three simulations provide reasonable distributions.

Now we make some comparisons between the fine-grid DES simulation, the DES-A simulation of Schmidt and Thiele [17], and the one-equation dynamic Smagorinsky LES of Sohankar et al. [15]. Comparisons of wake centerline quantities are made in Figs. 13 and 14. Figure 13 also includes the steady RANS results using the Spalart–Allmaras turbulence model obtained by Roy et al. [4]. The near-wake mean streamwise velocity predictions are comparable for the DES-A and LES simulations, whereas the LES does the better job of predicting the downstream recovery rate. The present fine-grid DES is most accurate in the entire wake region, albeit the improvement in accuracy is bought with an increase in mesh points. The RANS calculation does a poor job of capturing the near-wake mixing process and, as a result, grossly overpredicts the length of the recirculation zone. The prediction of u'_{rms} is dead-on for the LES and very good for the coarse DES-A case, whereas the present fine-grid DES simulation gives somewhat high values in the near-wake. All three simulations give good results for v'_{rms}, although the Sohankar LES gives a peak value somewhat upstream of the peak in the experiment, consistent with the prediction of smaller recirculation zone. The LES gives a higher peak magnitude of w'_{rms} than the two DES simulations, although the LES and fine-grid DES both predict a double-peaked distribution (the DES-A distribution very close to $x/D = 0.5$ was not decipherable from the given plot). Overall, the fine-grid DES results are comparable in accuracy to the one-equation dynamic model LES for the quantities considered. One should keep in mind, however, that some quantities, particularly the Reynolds shear stress at $x/D = 1$, are apparently sensitive to the grid resolution and the DES prediction is not guaranteed to improve with increasing grid resolution.

C. Supersonic Flow Past an Axisymmetric Base

The second flow considered is the supersonic flow past a cylindrical sting of radius $R = 31.75$ mm, studied experimentally by Herrin and Dutton [23]. A two-dimensional slice of the problem geometry is pictured in Fig. 15, along with computed contours of

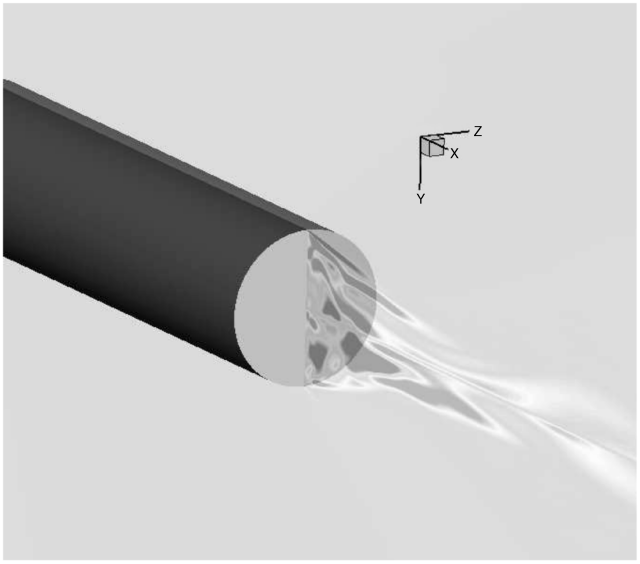

Fig. 15 Contours of streamwise vorticity in the wake of the axisymmetric base (fine grid).

Table 5 Flow conditions for the supersonic axisymmetric base problem

Parameter	Value
M_∞	2.46
u_∞	568.7 m/s
p_∞	3.208×10^4 Pa
T_∞	133 K
Re_R	1.65×10^6

Table 6 Simulation parameters for the supersonic axisymmetric base problem

Grid	N_{rz}	N_θ	N	$\Delta r_{\min}/R$	$\Delta r_{cl}/R$	$\Delta t/t_c$	T/t_c
Coarse	3250	48	156,000	4.9×10^{-5}	0.092	0.018	358.2
Fine	13,000	96	1,248,000	2.1×10^{-5}	0.064	0.018	447.8

streamwise vorticity. The flow separates from the sharp corner, turning through an expansion fan before recompressing downstream of the recirculation zone. The experimental freestream conditions, duplicated in the simulations, are given in Table 5.

Two simulation grids were constructed for this flow: a coarse grid, consisting of 156,000 cells, and a fine grid of 1,248,000 cells. The relevant parameters for the two grids are listed in Table 6. $\Delta r_{\min}$ is the mesh spacing in the radial direction at the corner, and Δr_{cl} is the radial mesh spacing at the center of the base. Both simulations were computed with the ACMSTVD scheme and $\kappa = 0.35$. Data were sampled at $x = -1$ mm in the boundary layer just upstream of the corner, on the base (pressure data), and along the wake centerline ($r = 0$). Simulation times are given in Table 6, and are normalized by the characteristic flow time $t_c = R/U_\infty$. The time step was chosen as 1.0×10^{-6} s based on temporal convergence studies of previous LES and DES simulations of this flow [24,25]. Adiabatic wall boundary conditions were applied along the surface of the sting.

Figure 16a compares the computed boundary layer velocity profile, scaled in the usual wall coordinates. The wall shear stress used to normalize each computational result was computed from the solution. Originally, the experimental profile was computed using an estimated theoretical shear stress reported in the experiment. This gives the previously reported velocity profile shown in the figure. Normalization using the fine-grid DES wall shear stress gives much better agreement between simulation and experiment, as shown. The first grid cell from the wall at this location had a $y+$ coordinate of 0.49 for the coarse grid and 0.19 for the fine grid. The simulations still predict a fuller velocity profile than the experimental profile at this location. This behavior is similar to unexplained discrepancies in the boundary layer reported by Forsythe et al. [24] and by Baurle et al. [25]. One possible cause of the discrepancy is simply insufficient grid resolution. Despite the well-resolved viscous sublayer, the present results indicate that the boundary layer solution may not be fully grid-converged. Nevertheless, the boundary layer thickness is close to the quoted experimental value of $\delta = 3.2$ mm. For the coarse grid, $\delta_{95} = 2.5$ mm and $\delta_{99} = 4.6$ mm, whereas for the fine grid, $\delta_{95} = 2.4$ mm and $\delta_{99} = 3.6$ mm.

Figure 16b compares the predicted base pressure coefficient with the experimental results. The coarse-grid result shows significant variation of the pressure across the base, although the mean value is close to the experiment. The fine grid gives a much more uniform distribution and is about 10% lower than the experimental value. The fine-grid results are very close to the DES results reported by Forsythe et al. [24] on a structured grid containing 2.6×10^6 cells.

Figure 17 shows the mean streamwise velocity and rms streamwise velocity fluctuation distributions along the wake centerline. The coarse grid grossly overpredicts the velocity deficit in the recirculation zone, but then agrees well with the data in the recovery region. The fine-grid solution agrees very well with the data

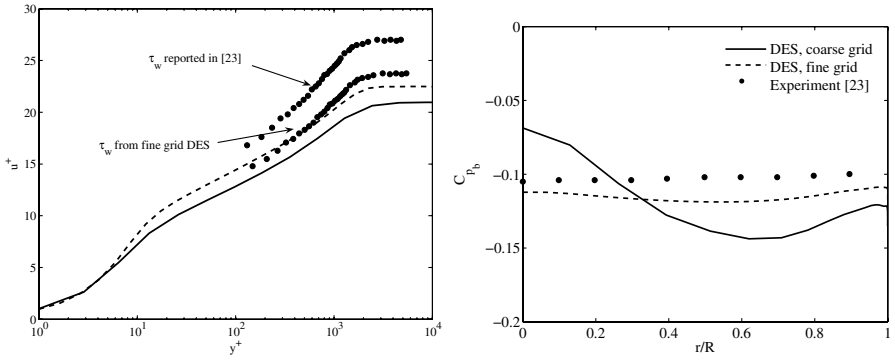

a) Velocity profile 1 mm upstream of base **b) Base pressure profile, predicted vs experimental data**

Fig. 16 Boundary layer velocity profile and base pressure profile.

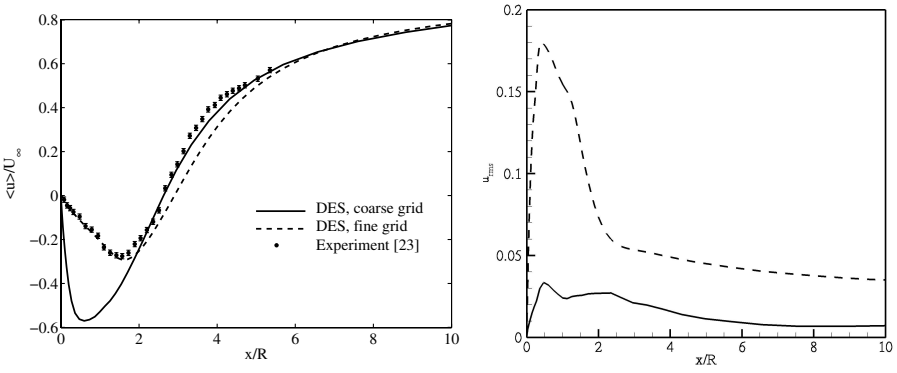

a) Mean velocity **b) RMS velocity**

Fig. 17 Mean and RMS streamwise velocity fluctuation for the axisymmetric base flow.

in the recirculation region, although giving a small underprediction of the velocity recovery. There are substantial differences in the rms velocity fluctuation levels on the two grids. It would be of interest to simulate this flow on a yet-finer grid, to both determine the level of solution convergence and examine if the agreement with the data improves uniformly with increasing resolution.

IV. Conclusions

The detached eddy simulation model was tested on two benchmark flow cases: the wake of a square cylinder and the supersonic wake of an axisymmetric base. Multiple grids were used in each problem, so that an assessment of solution improvement with increasing spatial resolution could be made. The numerical scheme employed was a variable-dissipation Roe scheme that used a characteristic-based switch to decrease dissipative error in smooth regions. The overall success of the present simulations using a (modified) dissipative flux scheme lends credence to the careful use of such schemes for unsteady simulation of turbulent flows.

Comparisons of the DES results to other LES simulations are generally favorable. Global quantities for the square cylinder wake are well predicted by DES, although care must be taken to ensure sufficient grid resolution. Mean flow properties are also well predicted in the near-wake of the square cylinder and the supersonic base. Prediction of second order turbulent statistics is generally good, although in some cases not very accurate even on a relatively fine grid. Care must be taken in assessing accuracy of these statistics, keeping in mind that the DES model reduces to direct numerical simulation in the limit of infinite grid resolution only in the LES region. The solution in the RANS region converges to a solution to the RANS model. Situations where thin turbulent layers in the RANS region pass data to the LES region, as with the shear layers of the square cylinder wake, may lead to model inaccuracies. Certainly, however, the DES model succeeds where RANS models often fail in predicting the mean flow and global flow quantities, and is currently a viable and affordable engineering tool.

Acknowledgments

The authors gratefully thank Ryan Bond and Larry DeChant of Sandia National Laboratories for reviewing this work and Jeff Payne, also from Sandia, for assisting with the simulations. Sandia is a multiprogram laboratory operated by Sandia Corporation, a Lockheed Martin Company for the United States Department of Energy's National Nuclear Security Administration under contract DEAC04- 94AL85000.

References

[1] Kline, S. J., Cantwell, B. J., and Lilley, G. M., *1980–81 AFOSR-HTTM-Stanford Conference on Complex Turbulent Flows Thermosciences Division*, Vol. 1, Stanford Univ., CA, 1981.

[2] Bradshaw, P., Launder, B. E., and Lumley, J. L., "Collaborative Testing of Turbulence Models (Data Bank Contribution)," *Journal of Fluids Engineering*, Vol. 118, No. 2, June 1996, pp. 243–247.

[3] Oberkampf, W. L., and Trucano, T. G., "Verification and Validation in Computational Fluid Dynamics," *Progress in Aerospace Sciences*, Vol. 38, No. 3, 2002, pp. 209–272.

[4] Roy, C. J., DeChant, L. J., Payne, J. L., and Blottner, F. G., "Bluff-Body Flow Simulations Using Hybrid RANS/LES," AIAA Paper 2003-3889, 2003.

[5] Yee, H. C., Sandham, N. D., and Djomehri, M. J., "Low-Dissipative High-Order Shock-Capturing Methods Using Characteristic-Based Filters," *Journal of Computational Physics*, Vol. 150, March 1999, pp. 199–238.

[6] Harten, A., "Artificial Compression Method for Computation of Shocks and Contact Discontinuities 3: Self-Adjusting Hybrid Schemes," *Mathematics of Computation*, Vol. 32, No. 142, April 1978, pp. 363–389.

[7] Wong, C. C., Blottner, F. G., Payne, J. L., and Soetrisno, M., "Implementation of a Parallel Algorithm for Thermo-Chemical Nonequilibrium Flow Solutions," AIAA Paper 95-0152, Jan. 1995.

[8] Wong, C. C., Soetrisno, M., Blottner, F. G., Imlay, S. T., and Payne, J. L., "PINCA: A Scalable Parallel Program for Compressible Gas Dynamics with Nonequilibrium Chemistry," Sandia National Lab., Rept. SAND 94-2436, Albuquerque, NM, April 1995.

[9] Yee, H. C., "Implicit and Symmetric Shock Capturing Schemes," NASA TM-89464, May 1987.

[10] Spalart, P. R., Jou, W.-H., Strelets, M., and Allmaras, S. R., "Comments on the Feasibility of LES for Wings, and on a Hybrid RANS/LES Approach," *Advances in DNS/LES, 1st AFOSR International Conference on DNS/LES*, Greyden Press, Columbus, OH, 1997, pp. 137–147.

[11] Spalart, P. R., and Allmaras, S. R., "One-Equation Turbulence Model for Aerodynamic Flows," *Recherche Aérospatiale*, Vol. 1, 1994, pp. 5–21.

[12] Lyn, D. A., Einav, S., Rodi, W., and Park, J.-H., "Laser-Doppler Velocimetry Study of Ensemble-Averaged Characteristics of the Turbulent Near Wake of a Square Cylinder," *Journal of Fluid Mechanics*, Vol. 304, Dec. 1995, pp. 285–319.

[13] Rodi, W., Ferziger, J., Breuer, M., and Pourquiè, M., "Status of Large-Eddy Simulations: Results of a Workshop," *Journal of Fluids Engineering*, Vol. 119, No. 2, 1997, pp. 248–262.

[14] Voke, P. R., "Flow Past a Square Cylinder: Test Case LES2," *Direct and Large Eddy Simulation 2*, edited by J. P. C. Challet, P. Voke, and L. Kouser, Kluwer, Dordrecht, The Netherlands, 1997.

[15] Sohankar, A., Davidson, L., and Norberg, C., "Large Eddy Simulation of Flow Past a Square Cylinder: Comparison of Different Subgrid Scale Models," *Journal of Fluids Engineering*, Vol. 122, March 2000, pp. 39–47.

[16] Fureby, C., Tabor, G., Weller, H. G., and Gosman, A. D., "Large Eddy Simulations of the Flow Around a Square Prism," *AIAA Journal*, Vol. 38, No. 3, 2000, pp. 442–452.

[17] Schmidt, S., and Thiele, F., "Comparison of Numerical Methods Applied to the Flow over Wall-Mounted Cubes," *International Journal of Heat Fluid Flow*, Vol. 23, No. 3, 2002, pp. 330–339.

[18] Maskell, E. C., "A Theory of the Blockage Effects on Bluff Bodies and Stalled Wings in a Closed Wind Tunnel," Reports and Memoranda 3400, Aeronautical Research Council, 1963.

[19] Norberg, C., "Flow Around Rectangular Cylinders: Pressure Forces and Wake Frequencies," *Journal of Wind Engineering and Industrial Aerodynamics*, Vol. 49, 1993, pp. 187–196.

[20] Bearman, P. W., and Obasaju, E. D., "Experimental Study of Pressure Fluctuations on Fixed and Oscillating Square-Section Cylinders," *Journal of Fluid Mechanics*, Vol. 119, June 1982, pp. 297–321.

[21] McLean, I., and Gartshore, C., "Spanwise Correlations of Pressure on a Rigid Square Section Cylinder," *Journal of Wind Engineering and Industrial Aerodynamics*, Vol. 41, 1993, pp. 797–808.

[22] Luo, S. C., Yazdani, M. G., Chew, Y. T., and Lee, T. S., "Effects of Incidence and Afterbody Shape on Flow Past Bluff Cylinders," *Journal of Wind Engineering and Industrial Aerodynamics*, Vol. 53, 1994, pp. 375–399.

[23] Herrin, J. L., and Dutton, J. C., "Supersonic Base Flow Experiments in the near Wake of a Cylindrical Afterbody," *AIAA Journal*, Vol. 32, No. 1, 1994, pp. 77–83.

[24] Forsythe, J. R., Hoffman, K. A., Cummings, R. M., and Squires, K. D., "Detached-Eddy Simulation with Compressibility Corrections Applied to a Supersonic Axisymmetric Base Flow," *Journal of Fluids Engineering*, Vol. 124, Dec. 2002, pp. 911–923.

[25] Baurle, R. A., Tam, C.-J., Edwards, J. R., and Hassan, H. A., "Hybrid Simulation Approach for Cavity Flows: Blending, Algorithm, and Boundary Treatment Issues," *AIAA Journal*, Vol. 41, No. 8, 2003, pp. 1463–1480.

D. Gaitonde
Associate Editor